Journal of Computational Physics 492 (2023) 112412

Contents lists available at ScienceDirect

Journal of Computational Physics

journal homepage: www.elsevier.com/locate/jcp

An efficient energy conserving semi-Lagrangian kinetic scheme for the Vlasov-Ampère system

Hongtao Liu [a,b], Xiaofeng Cai [c,d,*], Yong Cao [b], Giovanni Lapenta [a]

[a] Center for Mathematical Plasma Astrophysics, Department of Mathematics, KU Leuven, Leuven, 3001, Belgium
[b] School of Mechanical Engineering and Automation, Harbin Institute of Technology, Shenzhen, 518055, China
[c] Research Center of Mathematics, Advanced Institute of Natural Sciences, Beijing Normal University, Zhuhai, 519087, China
[d] Guangdong Provincial Key Laboratory of Interdisciplinary Research and Application for Data Science, BNU-HKBU United International College, Zhuhai, 519087, China

ARTICLE INFO

Article history:
Received 6 April 2023
Received in revised form 11 July 2023
Accepted 1 August 2023
Available online 16 August 2023

Keywords:
Plasma kinetic modeling
Semi-Lagrangian scheme
Vlasov-Ampère system
Energy conservation

ABSTRACT

In this paper, we present a novel kinetic scheme termed the Energy Conserving Semi-Lagrangian (ECSL) for the Vlasov-Ampère system. The novelty of the ECSL is that it retains the efficiency of the explicit scheme while simultaneously maintaining energy conservation and unconditional stability properties of the implicit scheme without relying on nonlinear iteration. The proposed ECSL method includes two main ingredients: the conservative Semi-Lagrangian (CSL) scheme and a novel field solver. The CSL scheme is utilized for the phase space discretization of the Vlasov equation, which enables the scheme to conserve mass exactly and remove the Courant-Friedrichs-Lewy restriction. The novel field solver is proposed by coupling the Ampère equation and the moments of the Vlasov equation in a semi-implicit way, allowing for an explicit and efficient calculation of the electric field. The combination of the novel field solver and CSL ensures that ECSL scheme conserves total energy and mass on the fully discrete level, regardless of spatial resolution and time step size. Moreover, the ECSL scheme still provides reliable solution even when its spatial and temporal resolution are insufficient to fully resolve the Debye length and plasma period, making it a promising tool for multiscale and lengthy simulations. Several numerical experiments are presented to demonstrate the accuracy, efficiency, and conservation properties of the proposed method.

1. Introduction

Plasma is crucial for various applications, including semiconductor processing, space propulsion, and magnetically confined fusion devices [1]. However, studying plasma behavior using traditional experimental methods is challenging due to its highly dynamic nature, prompting to the development of various simulation methods. Among these simulation methods, kinetic models, which begin with first principles and offer in-depth insights into the behavior of individual plasma particles, are particularly well-suited for comprehending the complex multi-scale plasma phenomena. This paper focuses on the Vlasov-Ampère (VA) model, which is one of fundamental kinetic models for collisionless electrostatic plasma.

* Corresponding author at: Research Center of Mathematics, Advanced Institute of Natural Sciences, Beijing Normal University, Zhuhai, 519087, China.
E-mail addresses: hongtao.liu@kuleuven.be (H. Liu), xfcai@bnu.edu.cn (X. Cai), yongc@hit.edu.cn (Y. Cao), giovanni.lapenta@kuleuven.be (G. Lapenta).

https://doi.org/10.1016/j.jcp.2023.112412
0021-9991/

To numerically solve the Vlasov equation in the context of the VA model, two main approaches can be employed: particle-based approach and grid-based approach. Particle in cell (PIC) is a well-known particle-based method that involves tracing the motion of a finite number of macro-particles [2]. While the PIC method is computationally efficient and suitable for high-dimensional problems [3–6], it can produce inherent numerical noise, particularly for plasma flows with small perturbations [7,8]. Alternatively, grid-based methods solve the kinetic equation directly in phase space and have been widely used in nonequilibrium neutral flows [9–15]. We refer to this method as the direct kinetic method (DKM). As a deterministic method, the DKM reduces numerical noise and allows for achieving high-order accuracy for phase space discretization, making it suitable for studying fine-scale details that are inaccessible to PIC.

Several efficient and accurate DKM solvers have been proposed for the Vlasov equation, including Eulerian or semi-Lagrangian finite difference [16–18], finite element [19–21], finite volume [22–26], and spectral methods [7,27,28]. Recent reviews of these methods can be found in [29–31]. In particular, the conservative semi-Lagrangian (CSL) scheme is noteworthy because it conserves mass exactly and can be free from the Courant-Friedrichs-Lewy (CFL) condition. Moreover, the conservative form of Vlasov equation allows the use of dimensional splitting to reduce multi-dimensional problems to a succession of one-dimensional problems. With dimensional splitting, the multi-dimensional, including 5D and 6D, semi-Lagrangian schemes have been developed for the Vlasov simulations [32–35]. Furthermore, several non-splitting schemes have also been proposed [36–38]. The focus of this paper is to develop an efficient, unconditionally stable and energy-conserving DKM solver for multidimensional electrostatic plasma.

Although most DKM methods preserve system mass and achieve high-order accuracy, the conservation of total energy has been not fully addressed. In lengthy simulations, numerical methods may create or eliminate spurious energy, leading to unphysical outcomes such as plasma self-heating or cooling [5]. This issue becomes more pronounced when under-resolved meshes or large time step sizes are used. To address this issue, Cheng et al. [39] provide an explicit Eulerian solver for VA that conserves total energy on the fully discrete level. More recently, Einkemmer et al. [40] proposed a mass, momentum, and energy conservative dynamical low-rank scheme for the Vlasov equation that modifies the Galerkin condition in a way that the equations of motion enforce the momentum equations, thus mimicking the structure of the original equation. This approach has also been applied to conservative low-rank algorithms for Vlasov dynamics [41]. In [42], Filbet and Xiong proposed a conservative discontinuous Galerkin method for the Vlasov-Poisson system using Hermite polynomials in the velocity space. Although these methods can exactly conserve energy, ensuring numerical stability still requires a well-resolved numerical time step size with respect to the plasma oscillation period. The necessity of resolving the smallest scales induced by plasma period, even if they are not of primary interest, makes these methods expensive for large-scale and multi-scale simulations [5].

Several implicit DKM solvers have been proposed to eliminate the restriction imposed by the plasma oscillation period while maintaining conservation of total energy. Cheng et al. [39] developed an implicit Eulerian solver for VA using implicit energy-conserving temporal discretizations. Anderson et al. [43] presented an implicit algorithm for the fully kinetic 1D-2V VA system that conserves mass, momentum, and energy up to a nonlinear convergence tolerance. To address the temporal stiffness introduced by the plasma period, the authors used high-order/low-order acceleration of the iterative implicit solver. More recently, Carrie et al. [44] proposed an unconditionally stable, time-implicit algorithm for the 1D Vlasov-Poisson system using the Crank-Nicolson discretization scheme and operator splitting for the Vlasov equation. This method conserves system mass and momentum exactly, but only approximately conserves energy. The authors also presented an unsplitting algorithm that exactly conserves energy, but still requires the use of nonlinear iterative solvers.

In this paper, we aim to address whether we can develop a scheme that retains the efficiency of explicit DKM while also preserving the benefits of implicit schemes, but without requiring nonlinear iteration. To the best of our knowledge, we present the first DKM solver that can achieve exact conservation of energy and unconditional stability while maintaining the desirable simplicity of explicit schemes. This is achieved using a new semi-Lagrangian scheme presented here, termed the Energy-Conserving Semi-Lagrangian (ECSL) method.

The proposed ECSL method is based on two main components: the CSL scheme and the novel field solver. Specifically, the CSL scheme is utilized for the phase space discretization of the Vlasov equation, enabling the method to remove the CFL restriction and conserve mass exactly. Specially, we proposed a novel field solver by semi-implicitly coupling the Ampère equation and the moments of the distribution function for plasma transport in the velocity space. This field solver, in combination with the CSL scheme, enables the proposed method to remove the numerical constraints caused by the Debye length and plasma period, as well as exactly conserve the total energy. Compared to the previous implicit DKM solver, the ECSL method does not require nonlinear iteration, resulting in a comparable numerical cost per time step to that of an explicit scheme. Furthermore, the ECSL method achieves second-order temporal accuracy using the Strang splitting method and can be generalized to higher orders. The method can also be generalized to multidimensional plasma simulations using the dimensional splitting procedures, which further enhance its efficiency. Finally, we present several numerical experiments to demonstrate the accuracy, stability, efficiency, and conservative properties of the ECSL method.

The rest of the paper is organized as follows. The Vlasov-Ampère (VA) system and its normalization are introduced in Section 2. In Section 3, the energy conserving semi-Lagrangian (ECSL) method is described in detail. We present the results of numerical studies in Section 4. Finally, a summary is given in Section 5.

2. The Vlasov-Ampère system

In this section, we recall the Vlasov-Ampère (VA) system and its equivalent form Vlasov-Poisson (VP) system. The VA or VP system is a first-principles representation of the electrostatic collisionless plasma. The evolution of particles can be described by the Vlasov equation,

$$\partial_t f_s + \boldsymbol{v}_s \cdot \nabla_{\boldsymbol{x}} f_s + \frac{q_s}{m_s} \boldsymbol{E} \cdot \nabla_{\boldsymbol{v}_s} f_s = 0 \,, \tag{1}$$

where $f_s = f_s(\boldsymbol{x}, \boldsymbol{v}, t)$ is the velocity distribution function for species s (s chooses e for electrons and i for ions) moving in d-dimensional velocity space with $\boldsymbol{v}_s$ at position $\boldsymbol{x}$ and time t. Here q_s and m_s are the species charge and mass, and ε is the permittivity. The electric field $\boldsymbol{E}$ can be obtained from the Ampère equation,

$$\varepsilon \partial_t \boldsymbol{E} + \boldsymbol{J} = 0 \,, \tag{2}$$

where $\boldsymbol{J} = \sum_s q_s n_s \boldsymbol{u}_s$ is the total current density, and $n_s \boldsymbol{u}_s = \int \boldsymbol{v}_s f_s d\boldsymbol{v}$ is the momentum for species s. Eqs. (1) and (2) are known as the VA system.

By taking the zeroth moment of the Vlasov equation (1) and summing over each species s, one can obtain the charge continuity equation,

$$\partial_t \rho + \nabla \cdot \boldsymbol{J} = 0 \,, \tag{3}$$

where $\rho = \sum_s q_s n_s$ is total charge density, and $n_s = \int f_s d\boldsymbol{v}$ is the number density for species s. Substituting Eq. (3) into Eq. (2), and defining the $\nabla\phi = -\boldsymbol{E}$, one can obtain,

$$-\varepsilon \Delta \phi = \rho. \tag{4}$$

Eq. (4) is known as the Poisson equation and ϕ is the electric potential. As a result, when the charge continuity equation (3) is satisfied, the VA system (1) and (2) is equivalent to VP system (1) and (4). In this paper, we focus on the VA system.

Without loss of generality, in this paper we consider the electrons dynamic with charge $-q$ and assume the ions with charge q form a uniform static background. It is well known that the Debye length λ and the electron plasma frequency ω_p are the characteristic spatial and temporal parameters for electrostatic plasma, which are receptively defined by

$$\lambda = \left(\frac{\varepsilon k_B T_e}{q^2 n_e}\right)^{1/2}, \quad \omega_p = \left(\frac{n_e q^2}{\varepsilon m_e}\right)^{1/2},$$

where k_B is the Boltzmann constant and T_e is the electron temperature.

We define the following dimensionless variables to normalize the VA system,

$$\begin{aligned} &\bar{x} = \frac{x}{x_0}, \bar{T} = \frac{T}{T_0}, \bar{m} = \frac{m}{m_0}, \bar{n} = \frac{n}{n_0}, \\ &\bar{v} = \frac{v}{v_0}, \ \bar{t} = \frac{t}{t_0}, \ \bar{f} = \frac{f}{f_0}, \ \bar{\boldsymbol{E}} = \frac{\boldsymbol{E}}{E_0}, \end{aligned} \tag{5}$$

where x_0, T_0, m_0 and n_0 are reference length, temperature, mass and number density, which are independent parameters. Besides, we choose the reference velocity $v_0 = \sqrt{k_B T_0 / m_0}$, time $t_0 = x_0 / v_0$, electric field $E_0 = k_B T_0 / q x_0$ and the distribution function $f_0 = n_0 / {v_0}^d$. Once the four parameters x_0, T_0, m_0 and n_0 are chosen, the dimensionless VA system will be determined.

In the current study, we let $T_0 = T_e$, $m_0 = m_e$, $n_0 = n_i$ unless otherwise stated. The reference length x_0 will be given in the specific simulation. Here we define the dimensionless Debye length $\bar{\lambda} = \lambda / x_0$. Accordingly, the dimensionless electron plasma frequency $\bar{\omega}_p = \omega_p t_0 = 1/\bar{\lambda}$. In the rest of paper, all variables are dimensionless unless stated otherwise, but we will drop the bar over the variables for simplicity. Then the VA system (1) and (2) can be written as

$$\partial_t f + \boldsymbol{v} \cdot \nabla_{\boldsymbol{x}} f - \boldsymbol{E} \cdot \nabla_{\boldsymbol{v}} f = 0, \tag{6}$$

$$\lambda^2 \partial_t \boldsymbol{E} + \boldsymbol{J} = 0 \,. \tag{7}$$

It should be noted that the subscript s of distribution function f is omitted in (6), since we only consider the electron dynamic. Similarly, the Poisson equation (4) can be normalized as

$$-\lambda^2 \Delta \phi = 1 - n, \tag{8}$$

which will be utilized to provide the initial electric field $\boldsymbol{E}$ in VA system (6) and (7).

It is well known that in principle the VA system conserves the total energy E_t

$$\mathrm{E}_t = \frac{1}{2}\int_{\Omega_x}\int_{\Omega_v} \boldsymbol{v}^2 f d\boldsymbol{v}d\boldsymbol{x} + \frac{\lambda^2}{2}\int_{\Omega_x} \boldsymbol{E}^2 d\boldsymbol{x},$$

where the first part is the kinetic energy E_K and the second is the electric energy E_E. Here, Ω_x represents the physics domain, and Ω_v represents the velocity domain. Besides, the total mass $\mathrm{L}_1 = \int_{\Omega_x}\int_{\Omega_v} f d\boldsymbol{v}d\boldsymbol{x}$ and momentum $\mathrm{P} = \int_{\Omega_x}\int_{\Omega_v} \boldsymbol{v} f d\boldsymbol{v}d\boldsymbol{x}$ of VA system should be conserved. However, it is challenging for numerical simulation to conserves the mass L_1, momentum P and total energy E_t of VA system simultaneously. On the other hand, in the traditional explicit kinetic solver, the numerical temporal and spatial step sizes $(\Delta x, \Delta t)$ of the method are restricted by the normalized Debye length λ due to the numerical stability.

In the following section, we aim to develop an efficient semi-implicit kinetic scheme for VA system (6) and (7), which not only exactly conserves the mass and total energy, but also is unconditional stable (its numerical parameter $(\Delta x, \Delta t)$ is free from λ).

3. Numerical methods

In this section, we will describe the proposed energy conserving semi-Lagrangian (ECSL) method for the VA system (6) and (7) and discuss its properties. The main components of the proposed method include the temporal discretizations in Section 3.1 and high-order spatial discretizations in Section 3.2. Then we present the conservative properties of the proposed ECSL in Section 3.3. Finally, the evolution procedure of the proposed method is presented in Section 3.4.

3.1. Temporal discretizations

In this section, we describe the temporal discretizations for the VA system (6) and (7), while considering $f(\boldsymbol{x}, \boldsymbol{v})$ and $\boldsymbol{E}(\boldsymbol{x})$ are continuous at the phase space and physical space respectively. To develop an efficient energy conserving kinetic scheme, we utilize the operator splitting algorithm to split the full VA system in two energy conserving subsystems. Then we present the explicit and fully implicit energy-conserving scheme for these subsystems. Finally, we develop a novel efficient exactly energy conserving semi-implicit scheme, which retains the efficiency of explicit scheme while preserving the stability of the fully implicit scheme.

Following [39], the full VA system can be split into two energy-conserving subsystems: the Hamiltonian $\mathcal{H}_f$ and Hamiltonian $\mathcal{H}_E$ system. The equations associated with the $\mathcal{H}_f$ system are given by

$$\begin{aligned} &\partial_t f + \boldsymbol{v}\cdot\nabla_{\boldsymbol{x}} f = 0,\\ &\partial_t \boldsymbol{E} = 0, \end{aligned} \tag{9}$$

while equations associated with the $\mathcal{H}_E$ system are given by

$$\begin{aligned} &\partial_t f - \boldsymbol{E}\cdot\nabla_{\boldsymbol{v}} f = 0,\\ &\lambda^2\partial_t \boldsymbol{E} = -\boldsymbol{J}. \end{aligned} \tag{10}$$

The physics behind $\mathcal{H}_f$ system (9) and $\mathcal{H}_E$ system (10) are well-defined, the former represents the particle transport in physical space, while the latter represents the interchange of particle acceleration in velocity space and electric fields. These two subsystems are similar to the Hamiltonian splitting in [45], but with slight differences in form. As both subsystems are energy-conserving, we just need to design an energy-conserving temporal discretizations for each subsystem and then carefully couple these two solvers to achieve the conservation in the entire VA system with desired accuracy.

With regards to the $\mathcal{H}_f$ system (9), any explicit Runge-Kutta or implicit method can be utilized to ensure energy conservation. This can be easily verified by taking the moments of f, but the details are omitted here. Instead, we provide a brief explanation in Section 3.3. Specially, we utilize the semi-lagrangian scheme,

$$f(\boldsymbol{x}, \boldsymbol{v}, t^{k+1}) = f(\boldsymbol{x} - \Delta t\boldsymbol{v}, \boldsymbol{v}, t^k), \tag{11}$$

where the temporal discretization is denoted by t^k for k-th time step. Obvious different from the explicit Runge-Kutta or implicit methods, the Eq. (11) is exact in time.

As for the $\mathcal{H}_E$ system (10), which constitutes the core coupling effect of the VA system, caution must be exercised in ensuring the energy conservation, i.e., the balance of kinetic and electric energy. Similar to [39], an explicit energy conserving scheme can be devised as follows,

$$\begin{aligned} &f^{k+1/2} = f^k + \tfrac{\Delta t}{2}\boldsymbol{E}^k\cdot\nabla_{\boldsymbol{v}} f^k,\\ &\lambda^2\boldsymbol{E}^{k+1} = \lambda^2\boldsymbol{E}^k + \Delta t\int \boldsymbol{v} f^{k+1/2} d\boldsymbol{v},\\ &f^{k+1} = f^k + \Delta t\boldsymbol{E}^{k+1/2}\cdot\nabla_{\boldsymbol{v}} f^{k+1/2}, \end{aligned} \tag{12}$$

where $\boldsymbol{E}^{k+1/2} = (\boldsymbol{E}^{k+1} + \boldsymbol{E}^{k})/2$. Obviously, the explicit scheme (12) is second order accurate in time. Despite being energy conserving and free from grid heating or cooling [5], similar to the conventional explicit scheme in plasma kinetic simulation, the numerical parameter in scheme (12) should be smaller than the normalized Debye length λ due to the stability restriction.

To remove the above stability restriction, a full implicit energy-conserving form can be easily utilized as follows:

$$\begin{aligned} &f^{k+1} - f^{k} - \Delta t \boldsymbol{E}^{k+1/2} \cdot \nabla_{\boldsymbol{v}} f^{k+1/2} = 0, \\ &\lambda^2 \left(\boldsymbol{E}^{k+1} - \boldsymbol{E}^{k}\right) = -\Delta t \boldsymbol{J}^{k+1/2}, \end{aligned} \tag{13}$$

where $\boldsymbol{J}^{k+1/2} = (\boldsymbol{J}^{k+1} + \boldsymbol{J}^{k})/2$. The scheme (13) is also energy conserving [39], but it leads to the nonlinear coupling between f and $\boldsymbol{E}$. Even though advanced algorithms such as the Jacobian-free Newton-Krylov method [46] are available for solving nonlinear equations, the numerical intensity of solving systems (13) still persists, especially in high dimension simulations.

To preserve advantages of both the explicit scheme (12) and implicit scheme (13), here we propose a novel efficient energy conserving semi-implicit kinetic scheme, termed ECSL. The main idea is based on two main ingredients: the coupling of the particles acceleration and electric field by using the moments of the Vlasov equation, and the implementation of the CSL scheme. On the one hand, both scheme (12) and (13) suggest that $\boldsymbol{E}^{k+1/2}$ should be used to achieve the energy conservation. If $\boldsymbol{E}^{k+1/2}$ is given, the distribution function $f(\boldsymbol{x}, \boldsymbol{v}, t^{k+1})$ can be accurately obtained using the CSL scheme,

$$f(\boldsymbol{x}, \boldsymbol{v}, t^{k+1}) = f(\boldsymbol{x}, \boldsymbol{v} + \Delta t \boldsymbol{E}^{k+1/2}, t^{k}). \tag{14}$$

The challenge now lies in obtaining $\boldsymbol{E}^{k+1/2}$. On the other hand, inspirited by [26], by taking the first moment of the first equation of system (13) or (10), and incorporating the Ampère equation, we obtain a linear system as follows,

$$\begin{aligned} &\boldsymbol{J}^{k+1} = \boldsymbol{J}^{k} + \Delta t \boldsymbol{E}^{k+1/2} n^{k+1/2}, \\ &\lambda^2 \boldsymbol{E}^{k+1} = \lambda^2 \boldsymbol{E}^{k} - \Delta t \boldsymbol{J}^{k+1/2}, \end{aligned} \tag{15}$$

where $n^{k+1/2} = n^{k}$ since $n^{k+1} = n^{k}$ holds true for system (10). This can be easily verified by taking the zeroth moment of system (10). From a physics perspective, electric fields only impact the velocity of particles but not their mass. It should be noted that the first equation in system (15) holds true without any approximations.

By solving the linear system (15), we can easily obtain the $\boldsymbol{E}^{k+1}$ as follows,

$$\boldsymbol{E}^{k+1} = \frac{\lambda^2 - \delta}{\lambda^2 + \delta} \boldsymbol{E}^{k} - \frac{\Delta t}{\lambda^2 + \delta} \boldsymbol{J}^{k}, \tag{16}$$

where $\delta = \frac{1}{4} n^{k} \Delta t^2$. Accordingly, we can easily obtain $\boldsymbol{E}^{k+1/2}$

$$\boldsymbol{E}^{k+1/2} = \frac{\lambda^2}{\lambda^2 + \delta} \boldsymbol{E}^{k} - \frac{\Delta t}{2\lambda^2 + 2\delta} \boldsymbol{J}^{k}. \tag{17}$$

Thanks the using of CSL (14) and linear system (15), the current ECSL is energy conserving, as will be demonstrated in Section 3.3.

Finally, we use $\mathcal{H}_f(\Delta t)$ to denote the scheme (11) for system (9), and $\mathcal{H}_E(\Delta t)$ to denote the scheme (14) and (15) for system (10). The $\mathcal{H}_f(\Delta t)$ is exact in time due to the implementation of Eq. (11), while $\mathcal{H}_E(\Delta t)$ is second order in time since the system (15) is second order. As a result, we can obtain a second order scheme for the entire VA system by using the Strang splitting method as follows,

$$\mathcal{H}(\Delta t) = \mathcal{H}_f(\Delta t/2) \mathcal{H}_E(\Delta t) \mathcal{H}_f(\Delta t/2). \tag{18}$$

It's worth mentioning that the current second order scheme (18) can be generalized to a higher order, since it is symmetric in time. The extension of second order time reversible schemes into fourth order time symmetric schemes has been successfully demonstrated in [39,47].

3.2. Spatial discretizations

In this section, we present the CSL scheme for the spatial discretizations of Eq. (11) in $\mathcal{H}_f$ system (9) and Eq. (14) in $\mathcal{H}_E$ system (10). The Eqs. (11) and (14) can be further expressed in a unified form,

$$\partial_t f + \partial_x (af) = 0, \tag{19}$$

where a denotes as either velocity $\boldsymbol{v}$ in Eqs. (11) or electrostatic force $-\boldsymbol{E}$ in Eq. (14). The Eq. (19) is the linear hyperbolic equation that enables the design of a conservative scheme following the characteristics lines. Here we employ the CSL scheme [22,48], which is briefly reviewed as follows:

Firstly, we introduce a set of mesh points $\{x_{i+1/2}\}_{I_i}$ of the computational domain $[x_{\min}, x_{\max}]$, where $I_i = [x_{i-1/2}, x_{i+1/2}]$ are uniform numerical cells with centers $x_i = (x_{i-1/2} + x_{i+1/2})/2$ and cell sizes $\Delta x_i = x_{i+1/2} - x_{i-1/2}$. Tracking characteristic lines of the cell $[x_{i-1/2}, x_{i+1/2}]$ backward, we can find its upstream cell $[x_{i-1/2} - a\Delta t, x_{i+1/2} - a\Delta t]$, which is denoted as $[x^*_{i-1/2}, x^*_{i+1/2}]$. Accordingly, we have

$$\int_{x_{i-1/2}}^{x_{i+1/2}} f(x, t^{k+1})dx = \int_{x^*_{i-1/2}}^{x^*_{i+1/2}} f(x, t^k)dx\,. \tag{20}$$

Here we let each of the gird values to be equal the mean value over cell I_i,

$$f_i^k = \frac{1}{\Delta x}\int_{x_{i-1/2}}^{x_{i+1/2}} f(x, t^k)dx. \tag{21}$$

Then Eq. (20) can be further rewritten in the flux form,

$$f_i^{k+1} = f_i^k + F_{i-1/2} - F_{i+1/2}\,, \tag{22}$$

where $F_{i-1/2} = \frac{1}{\Delta x}\int_{x_{i-1/2}-a\Delta t}^{x_{i-1/2}} f^k dx$ and $F_{i+1/2} = \frac{1}{\Delta x}\int_{x_{i+1/2}-a\Delta t}^{x_{i+1/2}} f^k dx$.

Several CSL scheme can be used to calculate the flux $F_{i+1/2}$. In the case of $\varphi < 1$ and $a > 0$, if we consider the third order scheme [22],

$$F_{i+1/2} = \left(f_i^k + \frac{1}{6}(2-|\varphi|)(1-|\varphi|)\left(f_{i+1}^k - f_i^k\right) + \frac{1}{6}(1-|\varphi|)(1+|\varphi|)\left(f_i^k - f_{i-1}^k\right)\right)\varphi\,, \tag{23}$$

where $\varphi = a\Delta t/\Delta x$ is related to CFL condition. If we consider the fifth order scheme [18],

$$F_{i+1/2} = (w_1\mathcal{F}_1 + w_2\mathcal{F}_2 + w_3\mathcal{F}_3)\varphi, \tag{24}$$

where

$$\begin{aligned} w_1 &= \tfrac{1}{20}(2 + 3|\varphi| + \varphi^2),\\ w_2 &= \tfrac{1}{10}(6 + \ |\varphi| - \varphi^2),\\ w_3 &= \tfrac{1}{20}(6 - 5|\varphi| + \varphi^2), \end{aligned}$$

and

$$\begin{aligned} \mathcal{F}_1 &= \tfrac{1}{6}\left((\varphi^2 - 3|\varphi| + 2)f(i-2) + (-2\varphi^2 + 9|\varphi| - 7)f(i-1) + (\varphi^2 - 6|\varphi| + 11)f(i)\right),\\ \mathcal{F}_2 &= \tfrac{1}{6}\left((\varphi^2 - 1)f(i-1) + (-2\varphi^2 + 3|\varphi| + 5)f(i) + (\varphi^2 - 3|\varphi| + 2)f(i+1)\right),\\ \mathcal{F}_3 &= \tfrac{1}{6}\left((\varphi^2 + 3|\varphi| + 2)f(i) + (-2\varphi^2 - 3|\varphi| + 5)f(i+1) + (\varphi^2 - 1)f(i+2)\right). \end{aligned}$$

Note that the case of $a \le 0$ is mirror symmetric with respect to x_i of the above procedure, and for $\varphi \ge 1$, it can be handled with a whole grid shift followed by the cases of $\varphi < 1$. The flux limiter, such as the PP limiter and WENO limiter, can be employed in the transport equation for the physical space given by Eq. (11). However, these flux limiters cannot be used in the velocity space transport equation represented by Eq. (14), as this would violate energy conservation. Further explanation on this will be provided in Section 3.3. It should be noted that designing a strategy that ensures both positivity of f and energy conservation is a non-trivial challenge.

The implementation of schemes (23) and (24) ensures that the current ECSL scheme precisely conserves mass and energy with third and fifth spatial accuracy, respectively, as well being free from the CFL restriction. These claims will be verified through numerical tests in Section 4.1.

3.3. Properties of the ECSL

This section will demonstrate the conservation properties of the proposed ECSL and provide a brief comparison with other grid-based kinetic methods. Firstly, we will show that the ECSL exactly conserve the mass L_1 and total energy E_t for the whole VA system. To demonstrate the conservation properties of the proposed ECSL, we need to show that the mass and total energy of the system are conserved under the system $\mathcal{H}_f(\Delta t)$ system (9) using CSL scheme (11), as well as the $\mathcal{H}_E(\Delta t)$ system (10) using CSL scheme (14) and electric field (15).

Regarding the $\mathcal{H}_f(\Delta t)$ system (9) with CSL scheme (11), using Eq. (21) we can obtain that

$$\int_{\Omega_v}\int_{\Omega_x} f(x_i, v_j, t^{k+1})dxdv = \sum_i\sum_j f_{ij}^{k+1}\Delta x_i \Delta v_j, \tag{25}$$

where $i = 1, ...N_x$, $j = 1, ...N_v$ and Δx_i and Δv_j are the cell sizes in the physic and velocity space, respectively. For brevity, we consider the periodic boundary condition. Using the CSL scheme (22), one can obtain that

$$\begin{aligned}\sum_i f_i^{k+1}\Delta x_i &= \sum_i \left(f_i^k + F_{i-1/2}^k - F_{i+1/2}^k\right)\Delta x_i \\ &= \sum_i f_i^k \Delta x_i + \left(F_{1/2}^k - F_{N_x+1/2}^k\right)\Delta x_i \\ &= \sum_i f_i^k \Delta x_i,\end{aligned} \tag{26}$$

holds true for each particle with velocity v_j. As a result, the ECSL scheme exactly conserves the system mass,

$$\sum_i \sum_j f_{ij}^{k+1}\Delta x_i \Delta v_j = \sum_i \sum_j f_{ij}^k \Delta x_i \Delta v_j. \tag{27}$$

Similarly, one can easily obtain the conservation of momentum and energy,

$$\sum_i \sum_j \boldsymbol{v}_j f_{ij}^{k+1}\Delta x_i \Delta v_j = \sum_i \sum_j \boldsymbol{v}_j f_{ij}^k \Delta x_i \Delta v_j, \tag{28}$$

$$\sum_i \sum_j \boldsymbol{v}_j \boldsymbol{v}_j f_{ij}^{k+1}\Delta x_i \Delta v_j = \sum_i \sum_j \boldsymbol{v}_j \boldsymbol{v}_j f_{ij}^k \Delta x_i \Delta v_j. \tag{29}$$

The above analysis suggests that energy conservation can be easily achieved for plasma transport in the physical space. One can use any spatial and temporal discretization for the $\mathcal{H}_f(\Delta t)$ system (9) if mass conservation holds true, given that the particle velocity is independent of the integration of the distribution function in the physics space. This means that we can enhance the numerical stability and control numerical oscillations of the $\mathcal{H}_f(\Delta t)$ system (9) by utilizing the flux limiter and positivity-preserving limiter.

For the $\mathcal{H}_E(\Delta t)$ system (10) utilizing both CSL (14) and electric field (15), we can obtain the ECSL exactly conserve the system mass, similar to Eq. (27). To facilitate comprehension of the conservation of momentum and energy, we begin with Eq. (20) and define that

$$\boldsymbol{v}' = \boldsymbol{v} - q_e \boldsymbol{E}^{k+1/2}\Delta t, \tag{30}$$

following the characteristic line. Then we can demonstrate that the momentum,

$$\begin{aligned}\int_{\Omega_v} \boldsymbol{v} f\left(x, \boldsymbol{v}, t^{k+1}\right) d\boldsymbol{v} &= \int_{\Omega_v} \left(\boldsymbol{v}' + q_e \boldsymbol{E}^{k+1/2}\Delta t\right) f\left(x, \boldsymbol{v}', t^k\right) d\boldsymbol{v}' \\ &= \int_{\Omega_v} \boldsymbol{v}' f\left(x, \boldsymbol{v}', t^k\right) d\boldsymbol{v}' - n^k \Delta t \boldsymbol{E}^{k+1/2},\end{aligned} \tag{31}$$

is valid for each physical cell x_i. As a result, we can express the total momentum for the $\mathcal{H}_E(\Delta t)$ system (10) as follows,

$$\sum_i \sum_j \boldsymbol{v}_j f_{ij}^{k+1}\Delta x_i \Delta v_j = \sum_i \sum_j \boldsymbol{v}_j f_{ij}^{k+1}\Delta x_i \Delta v_j - \sum_i \Delta t n_i^k \boldsymbol{E}_i^{k+1/2}\Delta x_i. \tag{32}$$

Equation (32) reveals that the momentum supplied by the ECSL is conserved if $\int_{\Omega_x} n\boldsymbol{E}dx = 0$, which holds true for many well-known examples [39]. To ensure exact conservation of system momentum for a general case, one should consider the other technique [40,42–44]. Regarding the conservation of total energy, we have

$$\begin{aligned}\frac{1}{2}\int_{\Omega_v} \boldsymbol{v}\boldsymbol{v} f\left(x, \boldsymbol{v}, t^{k+1}\right) d\boldsymbol{v} &= \frac{1}{2}\int_{\Omega_v} \left(\boldsymbol{v}' + q_e \boldsymbol{E}^{k+1/2}\Delta t\right)^2 f\left(x, \boldsymbol{v}', t^k\right) d\boldsymbol{v}' \\ &= \frac{1}{2}\int_{\Omega_v} \boldsymbol{v}'^2 f\left(x, \boldsymbol{v}', t^k\right) d\boldsymbol{v}' + \int_{\Omega_v} q_e \boldsymbol{E}^{k+1/2}\Delta t \left(\boldsymbol{v}' + q_e \boldsymbol{E}^{k+1/2}\Delta t/2\right) f\left(x, \boldsymbol{v}', t^k\right) d\boldsymbol{v}' \\ &= \frac{1}{2}\int_{\Omega_v} \boldsymbol{v}'^2 f\left(x, \boldsymbol{v}', t^k\right) d\boldsymbol{v}' + \Delta t \boldsymbol{E}^{k+1/2} \boldsymbol{J}^{k+1/2},\end{aligned} \tag{33}$$

where $\boldsymbol{J}^{k+1/2} = \int_{\Omega_v} q_e \left(\boldsymbol{v}' + q_e \boldsymbol{E}^{k+1/2}\Delta t/2\right) f\left(x, \boldsymbol{v}', t^k\right) d\boldsymbol{v}'$ is obtained from the first equation of Eq. (15). Then the total kinetic energy E_k for the $\mathcal{H}_E(\Delta t)$ system (10) can be expressed as,

$$\frac{1}{2}\sum_i\sum_j \boldsymbol{v}_j\boldsymbol{v}_j f_{ij}^{k+1}\Delta x_i\Delta v_j = \frac{1}{2}\sum_i\sum_j \boldsymbol{v}_j\boldsymbol{v}_j f_{ij}^{k}\Delta x_i\Delta v_j + \sum_i \Delta t \boldsymbol{E}_i^{k+1/2}\boldsymbol{J}_i^{k+1/2}\Delta x_i. \tag{34}$$

Meanwhile, multiplying $\boldsymbol{E}_i^{k+1/2}$ by the Ampère equation yields,

$$\lambda^2\frac{\boldsymbol{E}_i^{k+1}-\boldsymbol{E}_i^{k}}{\Delta t}\boldsymbol{E}_i^{k+1/2} = -\boldsymbol{J}_i^{k+1/2}\boldsymbol{E}_i^{k+1/2}. \tag{35}$$

Then the derivation of the total electric energy E_E can therefore be calculated as follows,

$$\frac{\lambda^2}{2}\sum_i\left|\boldsymbol{E}_i^{k+1}\right|^2\Delta x_i - \frac{\lambda^2}{2}\sum_i\left|\boldsymbol{E}_i^{k}\right|^2\Delta x_i = -\sum_i \Delta t\boldsymbol{E}_i^{k+1/2}\boldsymbol{J}_i^{k+1/2}\Delta x_i. \tag{36}$$

Combining Eq. (34) and Eq. (36), we can see that the ECSL exactly conserves the total energy for the $\mathcal{H}_E(\Delta t)$ system (10).

$$\frac{1}{2}\sum_i\sum_j \boldsymbol{v}_j\boldsymbol{v}_j f_{ij}^{k+1}\Delta x_i\Delta v_j + \frac{\lambda^2}{2}\sum_i\left|\boldsymbol{E}_i^{k+1}\right|^2\Delta x_i = \frac{1}{2}\sum_i\sum_j \boldsymbol{v}_j\boldsymbol{v}_j f_{ij}^{k}\Delta x_i\Delta v_j + \frac{\lambda^2}{2}\sum_i\left|\boldsymbol{E}_i^{k}\right|^2\Delta x_i. \tag{37}$$

Note that Eq. (32) and Eq. (34) also can be derived from the discretized flux form Eq. (22). Additionally, to accurately reflect the energy conservation of ECSL, one should consider that the velocity space is large enough so that the distribution function at the boundary approaches zero, as indicated by Eq. (30) and Eq. (33).

As a result, we can conclude that the proposed ECSL exactly conserve the system mass and total energy for the whole VA system, as will be confirmed by the numerical experiments in Section 4. Now let we discuss some differences between the proposed ECSL and other grid-based kinetic schemes.

Compared to previous explicit Eulerian or Semi-Lagrangian schemes for electrostatic plasma simulation, the proposed ECSL not only conserves total energy but is also unconditionally stable. The energy conservation property ensures stability and the ability to predict physical results in lengthy simulations, while the unconditional stability property allows for large-scale and multi-scale simulations since the numerical parameters are not limited by the normalized Debye length or CFL condition. Several Semi-Lagrangian schemes [16,18,22,48,49] have been proposed for plasma simulation that overcome the CFL condition limitation on the numerical time step, and energy conserving schemes [40–42,50] have also been proposed. However, the numerical time step size of these methods is still limited by the plasma oscillation period. This limitation can be overcome by incorporating semi-implicitly or implicitly the coupling between particle transport and field transport. Following this idea, a few semi-implicit kinetic schemes have been proposed [25,26,51], but they do not conserve total energy. More recently, an energy-conserving kinetic method was proposed for the Vlasov-Maxwell system based on the regularized moment method [52]. Notably, when the magnetic field is absent, the method in [52] reduces to the VA system similar to Eq. (15) presented in this study, but constrained by the CFL condition. To the best of our knowledge, no explicit or semi-implicit grid-based kinetic scheme, particularly the semi-Lagrangian method, has achieved both unconditional stability and energy conservation, despite the existence of some energy-conserving and unconditionally stable semi-implicit particle methods [5,53].

On the other hand, few implicit grid-based Eulerian schemes have been proposed [39,43,44]. These implicit schemes are analogous to the implicit scheme (13), which is energy-conserving and unconditionally stable. However, the results obtained from implicit schemes require nonlinear iterations, making them more complex and difficult to implement. Additionally, the tolerance of the nonlinear iterations can affect the energy conservation of the scheme. The implicit schemes are also time-consuming, especially for high-dimensional simulations. In contrast, the proposed ECSL is a semi-implicit scheme and does not require nonlinear iterations due to its use of the coupling of the moments of the Vlasov equation and Ampère equation, as shown in Eq. (15). Furthermore, the current ECSL has the same numerical cost per time step as an explicit scheme.

Briefly, our proposed ECSL takes the best of both of the explicit and implicit scheme, preserving the efficiency and ease of implementation of the explicit scheme while retaining the energy conserving and unconditionally stable properties of the implicit scheme.

3.4. Algorithm

To enhance understanding of the proposed Energy Conserving Semi-Lagrangian (ECSL) method, we present its evolution procedure. The procedure begins with the initial distribution function f^k and electric field $\boldsymbol{E}^k$, and evolves the ECSL from time t^k to t^{k+1} as follows:

(1) Update the $\mathcal{H}_f(\Delta t/2)$ system (9) by solving the CSL scheme (11) using Lie Splitting in physical space.
  (a) Compute the third or fifth order physics flux using Eq. (23) or Eq. (24) in each physics direction;
  (b) Obtain the distribution function $f^{k+1,*}$ by Eq. (22) in each physical direction.
(2) Update the $\mathcal{H}_E(\Delta t)$ system (10) by solving the CSL scheme (14) using Lie Splitting in the velocity space.
  (a) Compute electric field $\boldsymbol{E}^{k+1}$ using Eq. (16), and $\boldsymbol{E}^{k+1/2}$ using Eq. (17), where the current density $\boldsymbol{J}^k$ is obtained by taking the moments of the distribution function from physical transport step (1);

Table 1
Particle acceleration: $\Delta t = 0.5(\Delta v/v_m)^{3/2}$. The L^2 error and convergence order in space using the third scheme (23).

V	$N_v = 32$		$N_v = 64$		$N_v = 128$		$N_v = 256$	
	L^2 error	Order	L^2 error	Order	L^2 error	Order	L^2 error	Order
f	1.01E-01	–	2.26E-02	2.16	3.34E-03	2.76	4.32E-04	2.95
E	9.62E-03	–	1.24E-03	2.95	1.55E-04	3.00	1.94E-05	2.99

Table 2
Particle acceleration: $\Delta t = 0.5(\Delta v/v_m)^{5/2}$. The L^2 error and convergence order in space using the fifth order scheme (24).

V	$N_v = 32$		$N_v = 64$		$N_v = 128$		$N_v = 256$	
	L^2 error	Order	L^2 error	Order	L^2 error	Order	L^2 error	Order
f	3.12E-02	–	1.84E-03	4.08	6.26E-05	4.88	1.97E-06	4.99
E	3.69E-04	–	1.09E-05	5.08	3.41E-07	5.00	1.07E-08	4.99

(b) Compute the velocity flux according to Eq. (23) or Eq. (24) in each velocity direction;
(c) Obtain the distribution function $f^{k+1,**}$ by Eq. (22) in each velocity direction.

(3) Update the $\mathcal{H}_f(\Delta t/2)$ system (9) to obtain the distribution function f^{k+1} by solving the CSL scheme (11) using Lie Splitting in physical space. Here, the distribution function f^k is initiated from the distribution function $f^{k+1,**}$ obtained in step (2).

It should be noted that the process of step (3) is similar to that of step (1), which is omitted for the sake of simplicity. The steps from (1) to (3) are repeated continuously until either the simulation time is up or the criteria are satisfied. Besides, the initial electric field is obtained by solving the Poisson equation.

4. Numerical experiments

This section presents four numerical experiments to validate the proposed ECSL. The experiments include particle acceleration (0D1V), nonlinear Landau damping (1D1V), two-stream instability (1D1V), and 2D2V plasma wave. The proposed ECSL is diagnosed using the time evolution of electrostatic energy $\mathrm{E_E}$, mass $\mathrm{L_1}$, and total energy $\mathrm{E_t}$. For comparison purposes, we also present two non-energy conserving schemes termed CSL-PE and CSL-AE, which combine the CSL scheme with Ampère equation (AE) Eq. (7) and Poisson equation (PE) Eq. (8), respectively. The evolution procedure of CSL-AE and CSL-PE is similar to that of ECSL, except for the electric field evaluation in step 2a. Specifically, CSL-AE uses the formula $\boldsymbol{E}^{k+1} = \boldsymbol{E}^k - \Delta t \boldsymbol{J}^k/\lambda^2$, while CSL-PE solves the PE using the finite element method [48] to calculate $\boldsymbol{E}^{k+1}$. For all simulations, unless otherwise stated, the normalized Debye length is set to $\lambda = 1$, and the time step is set to $\Delta t = C\Delta x_m/v_m$, where C is the CFL number, Δx_m is the minimum physical grid spacing, and v_m is the maximum discretized velocity. Besides, periodic boundary conditions are imposed on both physical space and velocity space.

4.1. Particle acceleration

In this section, the particle acceleration (0D1V) is presented to investigate the accuracy and the conservative property of the proposed ECSL. To simplify the analysis, we consider the motion of a negatively charged particle in a given electric field $E(t) = \sin(t)$ within the velocity space v. The analytic solution for the particle distribution function can be derived as,

$$f(v,t) = \frac{1}{\sqrt{\pi}} \exp[-(v - E(t))^2]. \tag{38}$$

In our simulation, we define the velocity space as the interval $[-v_m, v_m]$ and discretize it with a grid of size N_v. The time step is set to $\Delta t = C\Delta v/E_m$, where $\Delta v = 2v_m/N_v$ and $E_m = 1$. Here we run this problem up to $t = 4\pi$.

First, we test the spatial accuracy of the proposed ECSL. Table 1 shows the L^2 error and convergence order of the ECSL using the third order scheme described in Eq. (23). To ensure that the spatial and temporal accuracy orders are the same, here we set time step $\Delta t = 0.5(\Delta v/v_m)^{3/2}$ with $v_m = 6$. The third order convergence in space is clearly confirmed in Table 1. On the other hand, Table 2 shows the L^2 error and convergence order of the ECSL using the fifth order scheme Eq. (24) with $\Delta t = 0.5(\Delta v/v_m)^{5/2}$. As expected, the table confirms a fifth-order convergence in space.

Then we investigate the temporal accuracy of the proposed ECSL. Table 3 summarizes the L^2 error and convergence order in time for different variables V with $N_v = 128$. The table confirms that the ECSL preserves second-order accuracy in time, which is expected since the $E^{k+1/2}$ is used. It is worth noting that the error for ECSL with the third order scheme and fifth order scheme is almost identical, and for brevity, we only present the results using the former scheme in Table 3. The evaluation of L^2 error refers to [48].

Now we demonstrate the conservative property of the proposed ECSL. Unless otherwise stated, the remainder of the paper will only present results obtained using the scheme described in Eq. (23). Fig. 1 presents the time evolution of the

Table 3
Particle acceleration: $N_v = 128$. The L^2 error and convergence order in time.

V	$C = 0.5$		$C = 1$		$C = 2$		$C = 4$	
	L^2 error	Order	L^2 error	Order	L^2 error	Order	L^2 error	Order
f	1.45E-03	–	5.80E-03	2.00	2.31E-02	1.99	8.95E-02	1.95
E	3.31E-03	–	1.32E-02	1.99	5.28E-02	2.00	2.09E-01	1.98

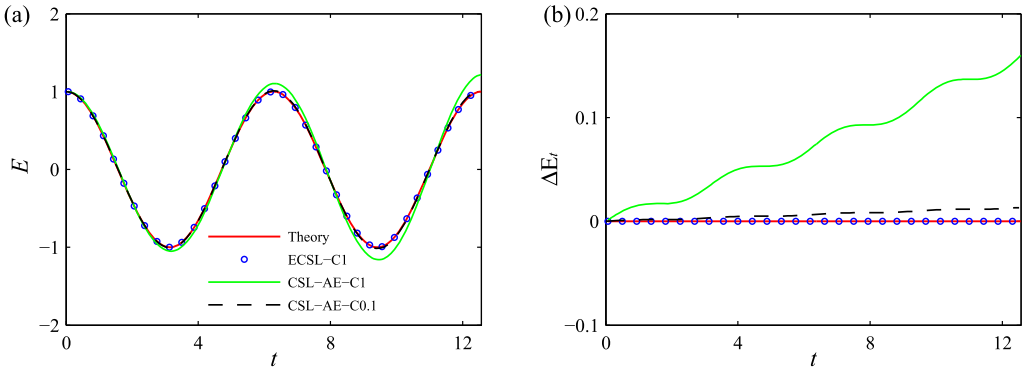

Fig. 1. Particle acceleration: $N_v = 128$. Time evolution of the electric field (a) and relative deviation of total energy (b).

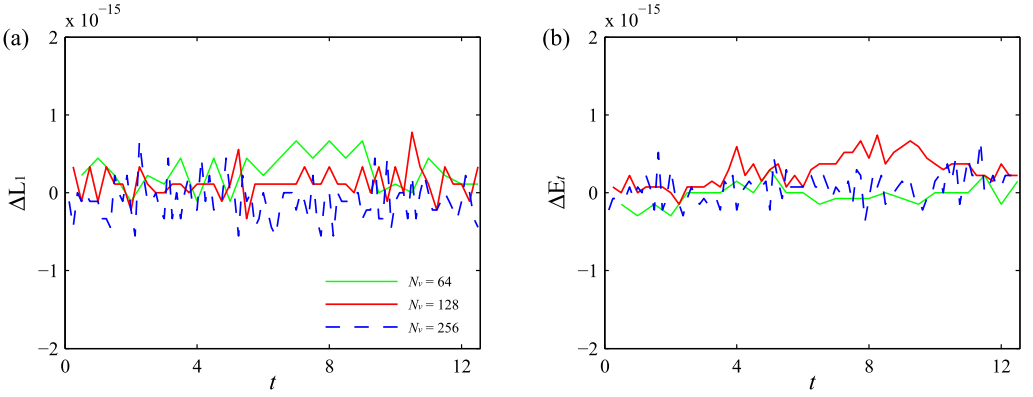

Fig. 2. Particle acceleration: $N_v = 128$, $C = 2$. Time evolution of the relative deviation of mass (a) and total energy (b).

electric field E, as well as the relative deviation of total energy $\Delta E_t = [E_t(t) - E_t(0)]/E_t(0)$ predicted by ECSL, CSL-AE, and the theoretical solution. It can be seen that the CSL-AE shows a significant deviation from the theoretical electric field E when using a CFL number of $C = 1$, resulting in a 20% increase in total energy. Although CSL-AE can predict the electric field more accurately using a smaller time step with $C = 0.1$, there is still a 2% increase in total energy. Encouragingly, the proposed ECSL not only accurately predicts the electric field with $C = 1$, but also exactly conserves the total energy. The contrasting results obtained by ECSL and CSL-AE suggest that considering the coupling of the moments of the Vlasov equation and Ampère equation, as described in Eq. (15), would yield more physically accurate results.

Furthermore, we would like to emphasize that to accurately reflect the conservation properties of our ECSL, v_m should be large enough to eliminate boundary effects, as discussed in Section 3.3. In our implementation, we have chosen $v_m = 8$. The conservation properties of the ECSL are not heavily reliant on the resolution of the velocity space. This is demonstrated in Fig. 2, where we present the time evolution of the relative deviation of mass $\Delta L_1 = [L_1(t) - L_1(0)]/L_1(0)$ and total energy ΔE_t with different grid sizes N_v in the velocity space, using a CFL number of $C = 2$. It is evident from the figure that the ECSL exactly conserves mass and total energy, even when a larger CFL number of $C = 2$ is used.

The above arguments indicate that the proposed ECSL is capable of achieving third and fifth-order accuracy in space using schemes (23) and (24), respectively, and second-order accuracy in time. Moreover, the ECSL ensures exact conservation of mass and total energy for plasma transport in velocity space. It should be noted that the proposed ECSL can be generalized to achieve higher-order spatial accuracy.

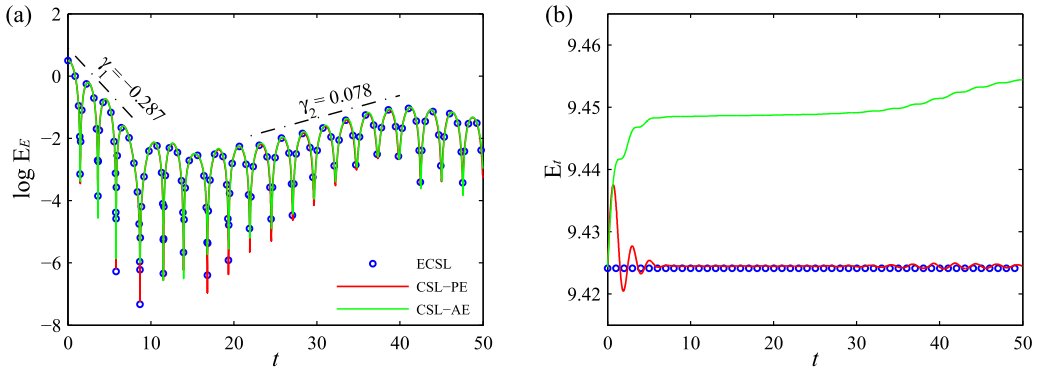

Fig. 3. Nonlinear landau damping: $C = 1$. Time evolution of the electric energy (a) and the total energy (b).

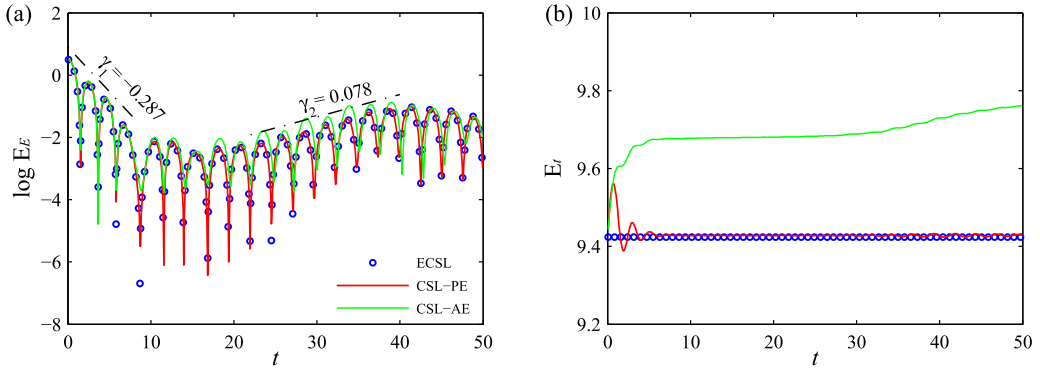

Fig. 4. Nonlinear landau damping: $C = 10$. Time evolution of the electric energy (a) and the total energy (b).

4.2. Nonlinear Landau damping

The proposed ECSL is now applied to simulate the nonlinear Landau damping for two main purposes. The first is to investigate the conservative properties of the proposed ECSL for the whole VA system, as compared to the CSL-AE and CSL-PE methods. The second is to investigate the effects of resolution of the physics space on the conservative property.

The initial condition for the simulation of the nonlinear Landau damping is given by

$$f(x, v) = \frac{1}{\sqrt{2\pi}}[1 + \alpha\cos(kx)]\exp(-v^2/2), \tag{39}$$

with $\alpha = 0.5$ and $k = 0.5$. In our simulation, the phase space domain is set to be $[0, L] \times [-v_m, v_m]$, where $L = 2\pi/k$ and $v_m = 9$. The phase grids are chosen as $N_x = 180$ and $N_v = 180$, unless otherwise stated. The simulation is run up to a final time of $t = 50$.

First, we investigate the energy conservation performance of the ECSL in comparison with the CSL-AE and CSL-PE. Fig. 3 shows the time evolution of the electric energy $\log E_E$ and the total energy E_t with a CFL number of $C = 1$. As shown in Fig. 3 (a), all schemes predict almost identical electric fields, as well the decay rate ($\gamma_1 = -0.287$) and growth rate ($\gamma_2 = 0.078$) of electric energy are consistent with the results in Ref. [10,19]. However, the three methods have different performances in terms of energy conservation. As shown in Fig. 3 (b), the CSL-AE method has a worse energy conservation performance, as the system's energy increases over time, resulting in a 0.3% energy increase at $t = 50$. On the other hand, the CSL-PE method has a larger deviation in energy initially, but it still maintains good energy conservation with an error on the order of 10^{-5} at $t = 50$. Encouragingly, the proposed ECSL exactly conserves the total energy.

The disparities among ECSL, CSL-AE, and CSL-PE become more pronounced when a larger CFL number of $C = 10$ is employed. Fig. 4 shows that CSL-AE produces a higher electric energy than ECSL and CSL-PE, resulting in a 3% energy increase. CSL-PE, on the other hand, provides almost the same electric energy as ECSL but still maintains energy conservation with an error on the order of 10^{-3}. Once again, the proposed ECSL ensures the exact conservation of total energy. One possible reason for the difference in energy conservation performance between the CSL-AE and CSL-PE methods is that the PE is a global equation, while the AE is local. Although the AE is more computationally efficient as it does not require solving a linear global matrix, it is less accurate. This may explain why the PE is more commonly used in electrostatic plasma simulations. Encouragingly, the ECSL method can achieve the same high accuracy as CSL-PE while maintaining the

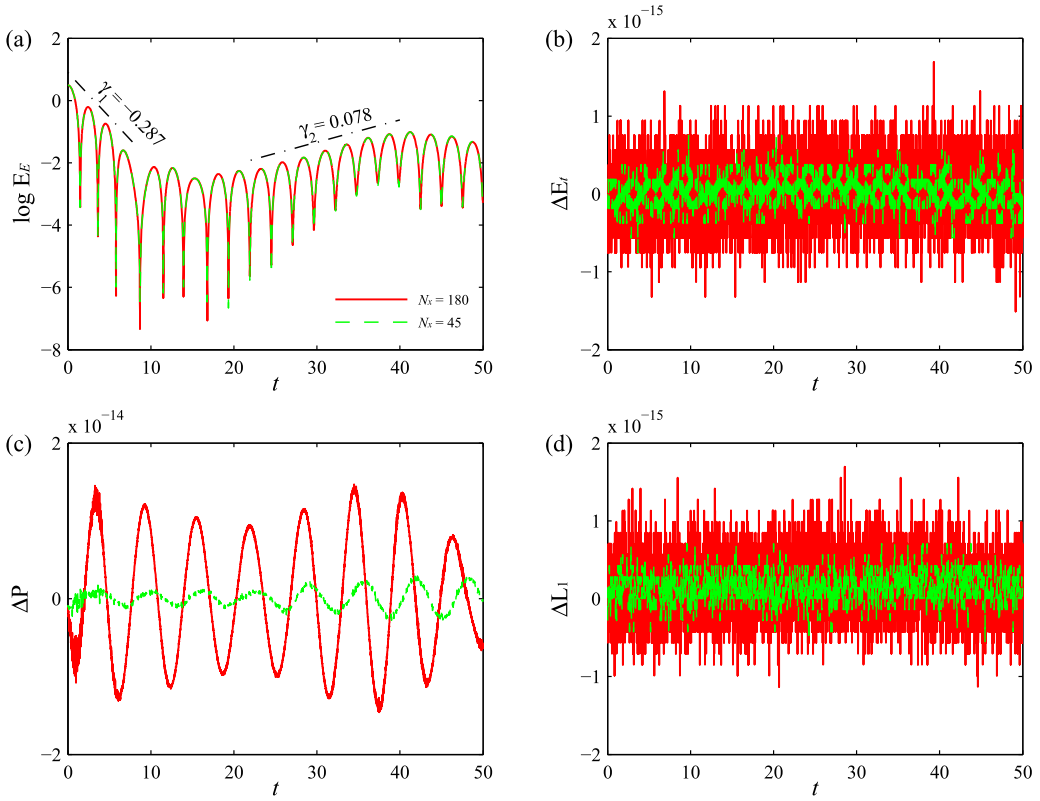

Fig. 5. Nonlinear landau damping: $C = 1$. Time evolution of the electric energy (a), relative deviation of total energy (b), absolute deviation of momentum (c) and relative deviation of mass (d) with different physical grids N_x.

computational efficiency of CSL-AE. This is mainly owing to the appropriate coupling of the moments of the Vlasov equation and AE which also ensures the exact conservation of total energy.

Then, we investigate the conservation performance of ECSL using the different physics gird sizes of N_x. Fig. 5 illustrates the time evolution of the electric energy, relative deviation of total energy, as well as deviation of total momentum ΔP and relative deviation of mass ΔL_1 using a CFL number of $C = 1$. Fig. 5 (a) indicates that the ECSL can accurately predict an electric field using a coarse grid of $N_x = 45$ that is almost identical to the one produced by a finer grid of $N_x = 180$. Additionally, both simulations are exactly conserved in total energy and mass for the whole VA system. The momentum conservation is also preserved in this simulation by the ECSL. The simulation results confirm the discussion presented in Section 3.3, where it was noted that the physics space discretization has no effect on the conservation properties of ECSL.

It is worth noting that the high-order CSL scheme employed by ECSL allows for accurate prediction of microscopic distribution function even with a coarse grid of $N_x = 45$, as shown in Fig. 6. In addition, we also would point out that flux limiters can be incorporated into physics space discretization process without compromising the conservation properties of the ECSL. This allows for greater flexibility in the choice of numerical schemes used in simulations, while still maintaining the accuracy and stability of the ECSL. The results with flux limiter are almost same as those of in Fig. 5, thus we have chosen not to present these results here for brevity.

The above arguments indicate that the proposed ECSL ensures exact conservation of mass and total energy for the whole VA system. Additionally, the conservation properties of the ECSL method are independent of the resolution of the physics space, as evidenced by the simulation results. Furthermore, the high-order CSL scheme employed by the ECSL enables accurate and efficient plasma simulations, making it a powerful tool for conducting accurate and efficient plasma simulations.

4.3. Two stream instability

In this section, we utilize the ECSL to simulate the two-stream instability and aim to explore the accuracy and conservation properties of the proposed ECSL for the entire VA system using a large time step. Specifically, we will investigate whether the ECSL can conserve the total energy even when the plasma oscillation period (equivalent to the normalized Debye length λ) is not well-resolved by the numerical time step.

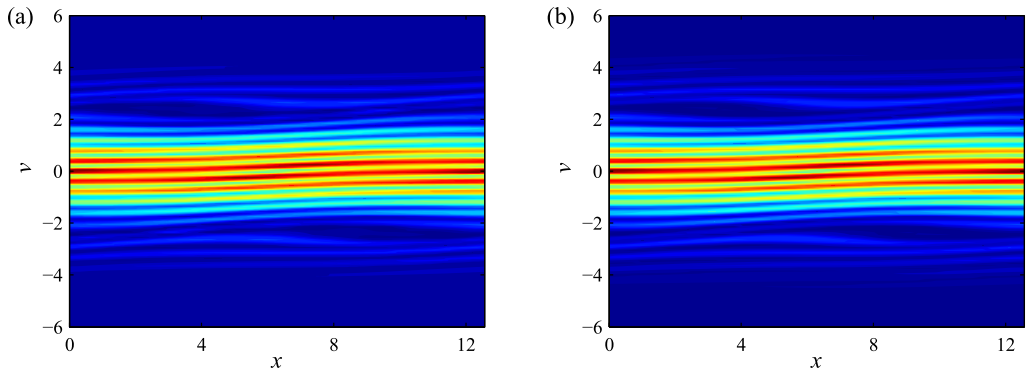

Fig. 6. Nonlinear landau damping: $C = 1$. Phase space plot of the velocity distribution function at $t = 50$ with fine grids $N_x = 180$ (a) and $N_x = 45$ (b).

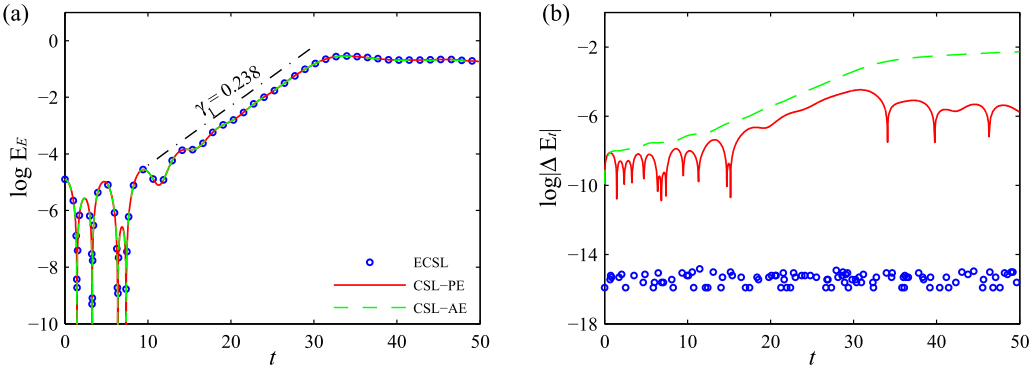

Fig. 7. Two stream instability: $\lambda = 1$, $C = 1$. Time evolution of the electric energy (a) and relative deviation of total energy (b).

The initial condition for the simulation of the two stream instability is given by

$$f(x, v) = \frac{1}{2\sqrt{2\pi}\, v_t}[1 + \alpha\cos(kx)]\left[\exp(-(v - v_0)^2/2v_t^2) + \exp(-(v + v_0)^2/2v_t^2)\right], \tag{40}$$

with $\alpha = 10^{-3}$, $k = 0.5$, $v_0 = 1.0$ and $v_t = 0.4$. In our simulation, the phase space domain is set to be $[0, L] \times [-v_m, v_m]$, where $L = 2\pi/k$ and $v_m = 6$. The phase grids are chosen as $N_x = 256$ and $N_v = 256$, unless otherwise stated. The simulation is run up to a final time of $t = 50$.

First, we investigate the accuracy of the proposed ECSL. Fig. 7 presents the time evolution of the electric energy and relative deviation of total energy predicted by ECSL using $C = 1$, together with the CSL-AE and CSL-PE solutions. As shown in Fig. 7 (a), all of the methods accurately predicted the electric energy, where the growth rate agrees well with the dispersion relation obtained from linear theory [54]. But only the ECSL exactly conserve the total energy, as shown in Fig. 7 (b). In contrast, the CSL-AE performs poorly on energy conservation, as the system's energy increases over time, resulting in a 2% energy increase. This observation once again highlights the significance of considering the coupling between particle transport and electric field if the AE is used for plasma simulation.

Then, we investigate the performance of the proposed ECSL when the large time step size is used. Fig. 8 illustrates the time evolution of the electric energy, relative deviation of total energy, as well as deviation of total momentum and relative deviation of mass using different CFL numbers. The use of the CSL scheme in the current implementation of the ECSL method not only eliminates the CFL constraint but also achieves greater accuracy by precisely tracking the trajectories of particles over time. As depicted in Fig. 8 (a), the ECSL with $C = 50$ produces nearly identical electric energy as the one with $C = 1$. Moreover, even with a large CFL number of $C = 50$, the total energy E_t and mass L_1 are conserved exactly, as demonstrated in Fig. 8 (b) and (d). Additionally, the momentum is also well conserved.

Fig. 9 presents the phase space plot of the velocity distribution function at $t = 50$ with the CFL number of $C = 1$ and $C = 10$. It can be seen that the microscopic structure captured by ECSL with $C = 10$ can be comparable to the results with $C = 1$, which demonstrates the high accuracy of the proposed method. The ability of the proposed method to predict accuracy results even with large time step sizes is a highly advantageous feature in the lengthy simulations.

It is crucial to note that even when $C = 50$ is used, the numerical time step $\Delta t = 0.41$ still accurately resolves plasma period $w_p^{-1} = \lambda = 1$. Therefore, CSL-PE and CSL-AE schemes remain stable in this case. However, if Δt fails to resolve the plasma oscillation period, both the CSL-PE and CSL-AE schemes become unstable due to their explicit nature [26]. On the other hand, the ECSL scheme still produces reliable results, as demonstrated in Fig. 10, which illustrates the time evolution

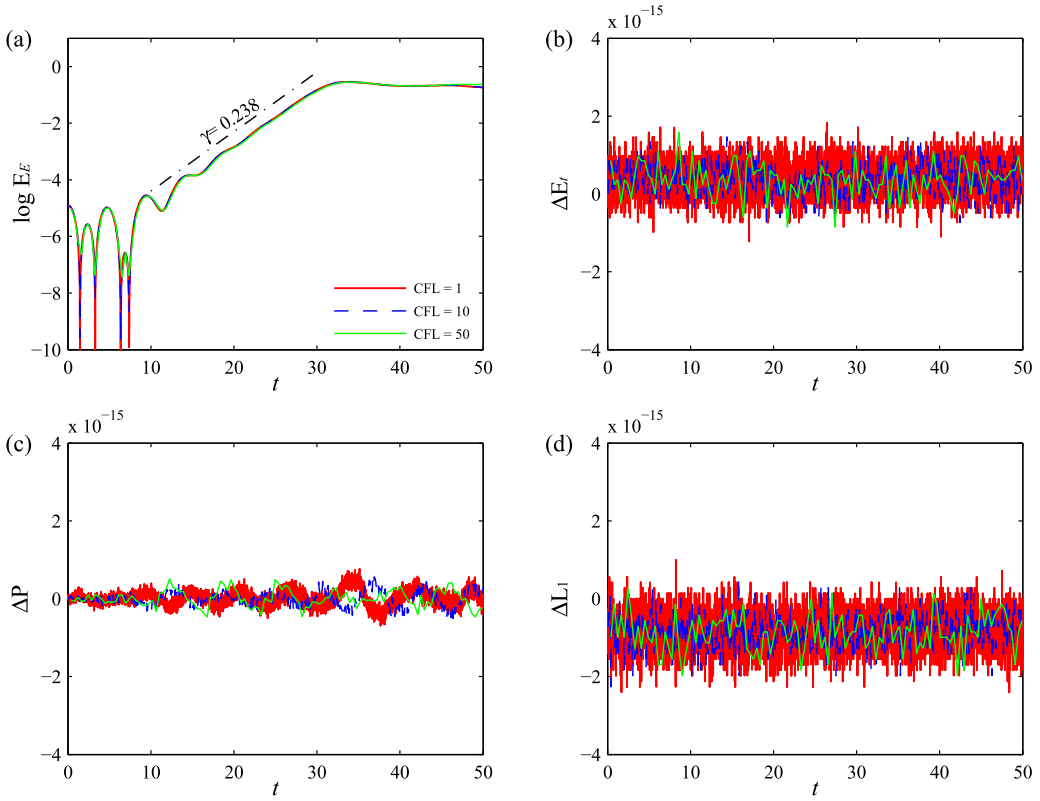

Fig. 8. Two stream instability: $\lambda = 1$, $C = 1, 10, 50$. Time evolution of the electric energy (a), relative deviation of total energy (b), absolute deviation of momentum (c) and relative deviation of mass (d) with different CFL numbers C.

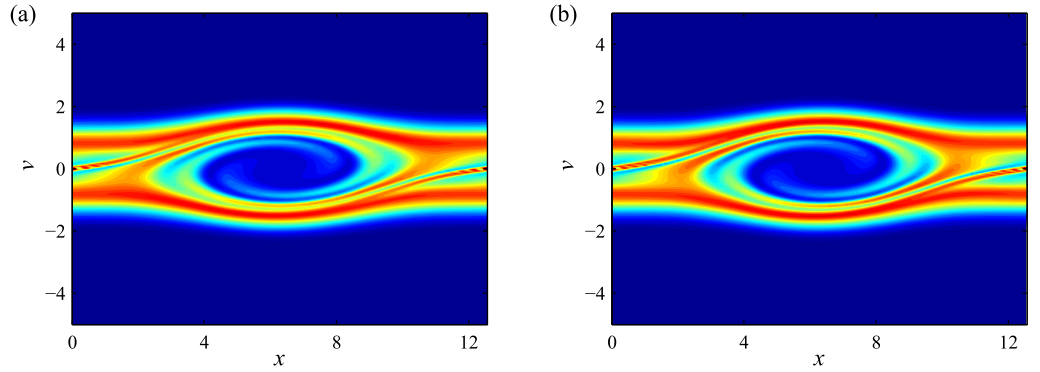

Fig. 9. Two stream instability: $\lambda = 1$, $C = 1, 10$. Phase space plot of the velocity distribution function at $t = 50$ with CFL number $C = 1$ (a) and $C = 10$ (b).

of the electric energy and the relative deviation of the total energy at different normalized Debye lengths λ. In Fig. 10 (a), the electric energy has been normalized by λ^2, with zero value replaced an extremely small value of 10^{-16}. The ECSL scheme predicts the results for $\lambda = 10^{-3}$ and $\lambda = 10^{-6}$, which are almost identical to those of the quasi-neutral limit ($\lambda = 0$). It should be emphasized that all simulations used a fixed grid spacing of $\Delta x = 0.05$ and a time step of $\Delta t = 0.008$, which is not limited by the normalized Debye length λ. The total energy is conserved exactly in all simulations, even when $\Delta t \gg \lambda$.

The above arguments demonstrate that the ECSL scheme is unconditionally stable and can produce accurate results even when using very large CFL numbers. Specifically, the ECSL can provide reliable results while exactly conserving the total energy even when the time step Δt is much larger than the normalized Debye length λ. This is particularly important for understanding complex plasma dynamics that involve different regimes. Traditional numerical methods typically require fine spatial and temporal resolutions to accurately capture small-scale dynamics. However, with the ECSL scheme, it is not necessary to resolve these small scales induced by λ, thereby reducing computational costs and enabling larger-scale simulations.

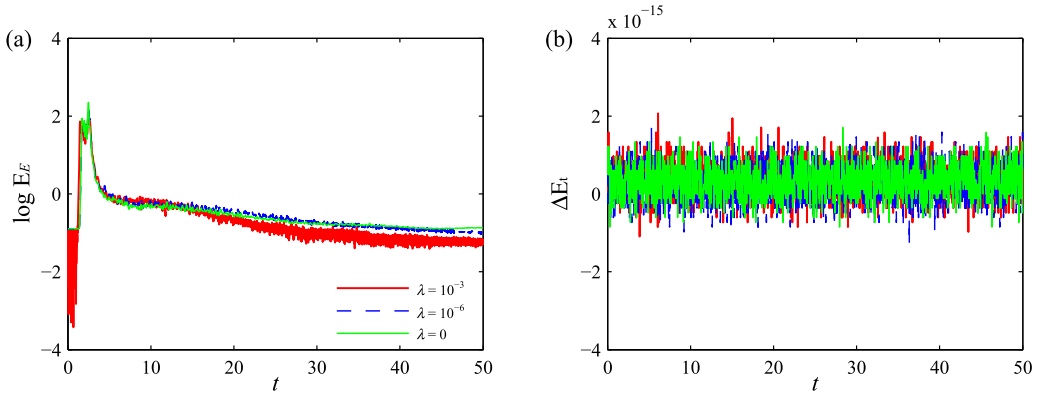

Fig. 10. Two stream instability: $C = 2$, $\lambda = 10^{-3}, 10^{-6}, 0$. Time evolution of the electric energy (a) and relative deviation of total energy (b) with different normalized Debye length λ.

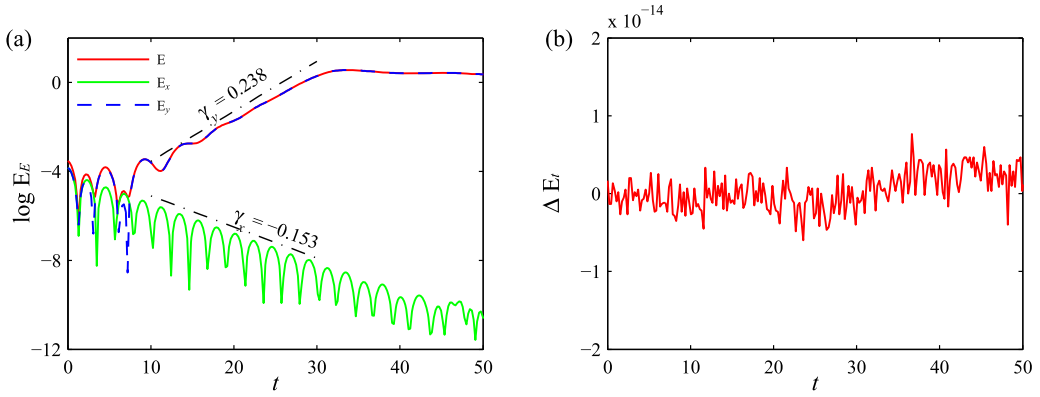

Fig. 11. 2D2V plasma wave: $C = 10$. Time evolution of the electric energy (a) and relative deviation of total energy (b).

4.4. 2D2V plasma wave

In this section, we will apply the ECSL scheme to a 2D2V electrostatic plasma wave simulation. The main purpose is to investigate the accuracy and conservation properties of the ECSL scheme in multidimensional simulations. The initial condition for the simulation of the 2D2V plasma wave is given by

$$f(x, y, v_x, v_y) = \frac{1}{4\pi v_{t_x} v_{t_y}}[1 + \alpha(\cos(k_x x) + \cos(k_y y))] f_{v_x} f_{v_y} \tag{41}$$

with $f_{v_x} = \exp(-|v_x|^2/2v_{t_x}^2)$, and $f_{v_y} = \exp(-(v_y - v_0)^2/2v_{t_y}^2) + \exp(-(v_y + v_0)^2/2v_{t_y}^2)$, where v_x and v_y are discrete velocity points.

In our simulation, we set the wavenumbers as $k_x = k_y = 0.5$, the thermal velocities as $v_{t_x} = 1.0$ and $v_{t_y} = 0.4$, and the drift velocity as $v_0 = 1$. The phase space domain is set to $[0, L_x] \times [0, L_y] \times [-v_{x_m}, v_{x_m}] \times [-v_{y_m}, v_{y_m}]$, where $L_x = 2\pi/k_x$, $L_y = 2\pi/k_y$, $v_{x_m} = 9$, and $v_{y_m} = 6$. We choose $N_x = N_y = 64$ and $N_{v_x} = N_{v_y} = 128$ as the phase space grid resolutions. The CFL number is set as $C = 10$, and the simulation is run up to a final time of $t = 50$. Here, we briefly present how to employ ECSL in 2D2V simulations. As shown in the algorithm in Section 3.4, we first update the $\mathcal{H}_f(\Delta t/2)$ system (9) using the CSL scheme with Lie Splitting. Specifically, $\mathcal{H}_f(\Delta t/2) = \mathcal{H}_{f_x}(\Delta t/2)\mathcal{H}_{f_y}(\Delta t/2)$, where $\mathcal{H}_{f_x}(\Delta t/2)$ and $\mathcal{H}_{f_y}(\Delta t/2)$ represents the particle transport (11) in x and y direction, respectively. Next, we update $\mathcal{H}_E(\Delta t) = \mathcal{H}_{E_E}(\Delta t)\mathcal{H}_{E_{v_x}}(\Delta t)\mathcal{H}_{E_{v_y}}(\Delta t)$, where $\mathcal{H}_{E_E}(\Delta t)$ represent the linear system (15) to obtain the electric field, $\mathcal{H}_{E_{v_x}}(\Delta t)$ and $\mathcal{H}_{E_{v_y}}(\Delta t)$, represent the particle transport (14) in v_x and v_y direction, respectively. Thirdly, we update $\mathcal{H}_f(\Delta t/2)$ system (9) again. This process continues until the desired simulation time is reached.

Fig. 11 shows the time evolution of the electric energy and the relative deviation of the total energy. In Fig. 11 (a), the expected linear Landau damping is observed in the x direction, while the expected two-stream instability is observed in the y direction. The decay rate of electric energy in the x direction and the growth rate of electric energy in the y direction predicted by ECSL both agree well with the linear theory [54]. Notably, ECSL conserves the total energy, as demonstrated in Fig. 11 (b).

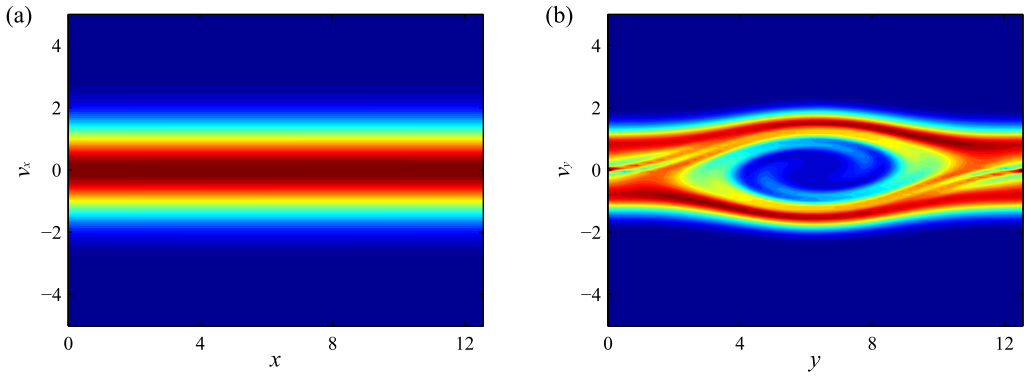

Fig. 12. 2D2V plasma wave: $C = 10$. Phase space plot of the velocity distribution function at $t = 50$ for $x - v_x$ cut at $y = L_y/2$ and $v_y = 0$ (a) and $y - v_y$ cut at $x = L_x/2$ and $v_x = 0$ (b).

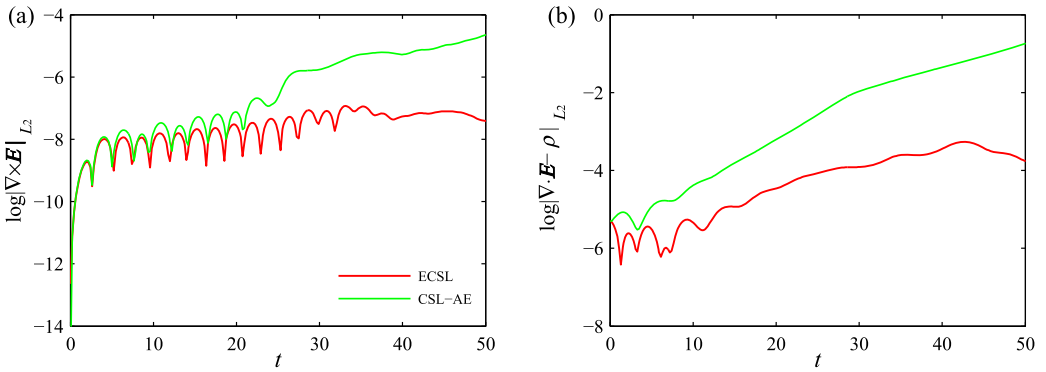

Fig. 13. 2D2V plasma wave: $C = 10$. Time evolution of curl error for electric field (a) and Gauss's law residual (b).

In Fig. 12, we also present the phase space plot the velocity distribution function for $x - v_x$ and $y - v_y$ cuts. The linear Landau damping and two-stream instability can be confirmed in the plot. These observations are consistent with the expected behavior of the system based on the linear theory, further validating the accuracy of the simulation results.

We further explore the time evolution of the curl error for electric field and the error for Gauss law, as illustrated in Fig. 13, where the error is measured using the L_2 norm averaged in the whole domain. Note that directly utilize the AE for multidimensional electrostatic simulation may result in a large curl error for electric field, as evident from Fig. 13 (a), where the curl error predicted by CSL-AE increases with time and reaches up to 10^{-4} at $t = 50$. Consequently, the error for Gauss law shown in Fig. 13 (b) becomes significant, approaching nearly 0.1. However, encouragingly, even though the primary goal of ECSL is to achieve total energy conservation and unconditional stability, it still preserves these two laws with small errors that do not grow with time. This suggests that ECSL would predict more reliable results in lengthy simulations.

The above arguments demonstrate that the proposed ECSL performs well in terms of accuracy and stability in multidimensional simulations, as well as its ability to precisely conserve total energy. Furthermore, the ECSL reduces multidimensional simulations to a series of one-dimensional problems, allowing for easy extension to multidimensional simulations while also making them more efficient and practical.

5. Conclusions

We have presented a novel grid-based kinetic solver, termed Energy Conserving Semi-Lagrangian (ECSL), for the Vlasov-Ampère system. The proposed method retains the efficiency of the explicit scheme and preserves the benefits of the implicit scheme. The key ingredients of ECSL include semi-implicit coupling of particle transport and electric field using the Vlasov equation moments, as well as exact tracking of particle trajectories in time by using conservative semi-Lagrangian methods. These key ingredients allow ECSL to conserve mass and total energy at the fully discrete level, regardless of spatial resolution and time step size. Additionally, the proposed method is unconditionally stable and can provide reliable results while maintaining exact conservation of total energy, even when the grid size and time step cannot resolve the Debye length and plasma period. Furthermore, the utilization of high-order CSL schemes allows for stable and accurate simulations, even with very large CFL numbers. It is important to note that the proposed ECSL has the same computational complexity and cost as the explicit scheme. We emphasize that our algorithm has been easily extended to multidimensional simulations, and also

can be generalized to higher orders in both space and time. As a result, the proposed ECSL provides a promising alternative for plasma simulations, especially in multiscale and lengthy simulations.

Further research is being conducted to build on the results presented above. For realistic 3D3V simulations, massive parallelization and memory reduction techniques are required. The proposed electrostatic field solver is advantageous over the Poisson solver in that it can be easily parallelized, resulting in a highly scalable algorithm suitable for exascale computing platforms. Additionally, further development of the current ECSL for electromagnetic plasma simulation will be presented in our near future work.

CRediT authorship contribution statement

Hongtao Liu: Conceptualization, Methodology, Software, Validation, Writing – original draft. **Xiaofeng Cai:** Methodology, Validation, Writing – review & editing. **Yong Cao:** Funding acquisition, Validation. **Giovanni Lapenta:** Funding acquisition, Resources, Supervision, Writing – review & editing.

Declaration of competing interest

The authors declared that they have no conflicts of interest to this work. We declare that we do not have any commercial or associative interest that represents a conflict of interest in connection with the work submitted.

Data availability

Data will be made available on request.

Acknowledgements

At KU Leuven, the work was supported by the KU Leuven Bijzonder Onder-zoeksfonds (BOF) under the C1 project TRACESpace, and by the European Union's project DEEP-SEA (Grant agreement 955606). This work was supported by a PostDoctoral Fellowship 1252224N from Research Foundation-Flanders (FWO). Cai was partially supported by National Natural Science Foundation of China [Grant Number 12201052], the Guangdong Provincial Key Laboratory of Interdisciplinary Research and Application for Data Science, project code 2022B1212010006, BNU-HKBU United International College. Additionally, this work received partial support from the Guangdong Basic and Applied Basic Research Foundation (No. 2023A1515010137) and Shenzhen Technology Project (No. ZDSYS201707280904031).

References

[1] F.F. Chen, Introduction to Plasma Physics and Controlled Fusion, vol. 1, Springer, 1984.
[2] C. Birdsall, A. Langdon, Plasma Physics via Computer Simulation, Taylor & Francis, 2004.
[3] S. Markidis, G. Lapenta, et al., Multi-scale simulations of plasma with iPIC3D, Math. Comput. Simul. 80 (2010) 1509–1519.
[4] G. Lapenta, Particle simulations of space weather, J. Comput. Phys. 231 (2012) 795–821.
[5] G. Lapenta, Exactly energy conserving semi-implicit particle in cell formulation, J. Comput. Phys. 334 (2017) 349–366.
[6] G. Lapenta, W. Jiang, Implicit temporal discretization and exact energy conservation for particle methods applied to the Poisson–Boltzmann equation, Plasma 1 (2018) 242–258.
[7] E. Camporeale, G.L. Delzanno, B. Bergen, J.D. Moulton, On the velocity space discretization for the Vlasov–Poisson system: comparison between implicit Hermite spectral and Particle-in-Cell methods, Comput. Phys. Commun. 198 (2016) 47–58.
[8] H. Liu, L. Quan, Q. Chen, S. Zhou, Y. Cao, Discrete unified gas kinetic scheme for electrostatic plasma and its comparison with the particle-in-cell method, Phys. Rev. E 101 (2020) 043307.
[9] K. Xu, J.-C. Huang, A unified gas-kinetic scheme for continuum and rarefied flows, J. Comput. Phys. 229 (2010) 7747–7764.
[10] Z. Guo, K. Xu, R. Wang, Discrete unified gas kinetic scheme for all Knudsen number flows: low-speed isothermal case, Phys. Rev. E 88 (2013) 033305.
[11] H. Liu, Y. Cao, Q. Chen, M. Kong, L. Zheng, A conserved discrete unified gas kinetic scheme for microchannel gas flows in all flow regimes, Comput. Fluids 167 (2018) 313–323.
[12] H. Liu, M. Kong, Q. Chen, L. Zheng, Y. Cao, Coupled discrete unified gas kinetic scheme for the thermal compressible flows in all Knudsen number regimes, Phys. Rev. E 98 (2018) 053310.
[13] J. Chen, S. Liu, Y. Wang, C. Zhong, Conserved discrete unified gas-kinetic scheme with unstructured discrete velocity space, Phys. Rev. E 100 (2019) 043305.
[14] T. Chen, X. Wen, L.-P. Wang, Z. Guo, J. Wang, S. Chen, Simulation of three-dimensional compressible decaying isotropic turbulence using a redesigned discrete unified gas kinetic scheme, Phys. Fluids 32 (2020) 125104.
[15] L. Yang, X. Zhao, C. Shu, Y. Du, Parametric reduced order modeling-based discrete velocity method for simulation of steady rarefied flows, J. Comput. Phys. (2020) 110037.
[16] C.-Z. Cheng, G. Knorr, The integration of the Vlasov equation in configuration space, J. Comput. Phys. 22 (1976) 330–351.
[17] J. Whealton, R. McGaffey, P. Meszaros, A finite difference 3-D Poisson-Vlasov algorithm for ions extracted from a plasma, J. Comput. Phys. 63 (1986) 20–32.
[18] T. Xiong, J.-M. Qiu, Z. Xu, A. Christlieb, High order maximum principle preserving semi-Lagrangian finite difference WENO schemes for the Vlasov equation, J. Comput. Phys. 273 (2014) 618–639.
[19] R.E. Heath, I.M. Gamba, P.J. Morrison, C. Michler, A discontinuous Galerkin method for the Vlasov–Poisson system, J. Comput. Phys. 231 (2012) 1140–1174.
[20] J.A. Rossmanith, D.C. Seal, A positivity-preserving high-order semi-Lagrangian discontinuous Galerkin scheme for the Vlasov–Poisson equations, J. Comput. Phys. 230 (2011) 6203–6232.

[21] J.-M. Qiu, C.-W. Shu, Positivity preserving semi-Lagrangian discontinuous Galerkin formulation: theoretical analysis and application to the Vlasov–Poisson system, J. Comput. Phys. 230 (2011) 8386–8409.
[22] F. Filbet, E. Sonnendrücker, P. Bertrand, Conservative numerical schemes for the Vlasov equation, J. Comput. Phys. 172 (2001) 166–187.
[23] J.W. Banks, J.A.F. Hittinger, A new class of nonlinear finite-volume methods for Vlasov simulation, IEEE Trans. Plasma Sci. 38 (2010) 2198–2207.
[24] J.-M. Qiu, A. Christlieb, A conservative high order semi-Lagrangian WENO method for the Vlasov equation, J. Comput. Phys. 229 (2010) 1130–1149.
[25] C. Liu, K. Xu, A unified gas kinetic scheme for continuum and rarefied flows V: multiscale and multi-component plasma transport, Commun. Comput. Phys. 22 (2017) 1175–1223.
[26] H. Liu, F. Shi, J. Wan, X. He, Y. Cao, Discrete unified gas kinetic scheme for a reformulated BGK-Vlasov-Poisson system in all electrostatic plasma regimes, Comput. Phys. Commun. (2020) 107400.
[27] J.W. Schumer, J.P. Holloway, Vlasov simulations using velocity-scaled Hermite representations, J. Comput. Phys. 144 (1998) 626–661.
[28] S. Le Bourdiec, F. De Vuyst, L. Jacquet, Numerical solution of the Vlasov–Poisson system using generalized Hermite functions, Comput. Phys. Commun. 175 (2006) 528–544.
[29] T. Arber, R. Vann, A critical comparison of Eulerian-grid-based Vlasov solvers, J. Comput. Phys. 180 (2002) 339–357.
[30] F. Filbet, E. Sonnendrücker, Comparison of Eulerian Vlasov solvers, Comput. Phys. Commun. 150 (2003) 247–266.
[31] G. Dimarco, L. Pareschi, Numerical methods for kinetic equations, Acta Numer. (2014) 369–520.
[32] L. Einkemmer, A performance comparison of semi-Lagrangian Discontinuous Galerkin and spline based Vlasov solvers in four dimensions, J. Comput. Phys. 376 (2019) 937–951.
[33] T. Umeda, K. Togano, T. Ogino, Two-dimensional full-electromagnetic Vlasov code with conservative scheme and its application to magnetic reconnection, Comput. Phys. Commun. 180 (2009) 365–374.
[34] H. Schmitz, R. Grauer, Kinetic Vlasov simulations of collisionless magnetic reconnection, Phys. Plasmas 13 (2006) 092309.
[35] K. Kormann, K. Reuter, M. Rampp, A massively parallel semi-Lagrangian solver for the six-dimensional Vlasov–Poisson equation, Int. J. High Perform. Comput. Appl. 33 (2019) 924–947.
[36] N. Crouseilles, P. Glanc, S.A. Hirstoaga, E. Madaule, M. Mehrenberger, J. Pétri, A new fully two-dimensional conservative semi-Lagrangian method: applications on polar grids, from diocotron instability to itg turbulence, Eur. Phys. J. D 68 (2014) 1–10.
[37] X. Cai, W. Guo, J.-M. Qiu, A high order semi-Lagrangian Discontinuous Galerkin method for Vlasov–Poisson simulations without operator splitting, J. Comput. Phys. 354 (2018) 529–551.
[38] X. Cai, W. Guo, J.-M. Qiu, A high order semi-Lagrangian Discontinuous Galerkin method for the two-dimensional incompressible Euler equations and the guiding center Vlasov model without operator splitting, J. Sci. Comput. 79 (2019) 1111–1134.
[39] Y. Cheng, A.J. Christlieb, X. Zhong, Energy-conserving discontinuous Galerkin methods for the Vlasov–Ampère system, J. Comput. Phys. 256 (2014) 630–655.
[40] L. Einkemmer, I. Joseph, A mass, momentum, and energy conservative dynamical low-rank scheme for the Vlasov equation, J. Comput. Phys. 443 (2021) 110495.
[41] W. Guo, J.-M. Qiu, A conservative low rank tensor method for the Vlasov dynamics, arXiv:2201.10397, 2022.
[42] F. Filbet, T. Xiong, Conservative discontinuous Galerkin/Hermite spectral method for the Vlasov–Poisson system, Commun. Appl. Math. Comput. Sci. (2020) 1–26.
[43] S.E. Anderson, W.T. Taitano, L. Chacón, A.N. Simakov, An efficient, conservative, time-implicit solver for the fully kinetic arbitrary-species 1D-2V Vlasov-Ampère system, J. Comput. Phys. 419 (2020) 109686.
[44] M. Carrié, B. Shadwick, An unconditionally stable, time-implicit algorithm for solving the one-dimensional Vlasov–Poisson system, J. Plasma Phys. 88 (2022) 905880201.
[45] N. Crouseilles, L. Einkemmer, E. Faou, Hamiltonian splitting for the Vlasov–Maxwell equations, J. Comput. Phys. 283 (2015) 224–240.
[46] D.A. Knoll, D.E. Keyes, Jacobian-free Newton–Krylov methods: a survey of approaches and applications, J. Comput. Phys. 193 (2004) 357–397.
[47] J. De Frutos, J. Sanz-Serna, An easily implementable fourth-order method for the time integration of wave problems, J. Comput. Phys. 103 (1992) 160–168.
[48] H. Liu, X. Cai, G. Lapenta, Y. Cao, Conservative semi-Lagrangian kinetic scheme coupled with implicit finite element field solver for multidimensional Vlasov Maxwell system, Commun. Nonlinear Sci. Numer. Simul. 102 (2021) 105941.
[49] H. Liu, M. Chen, X. Cai, Y. Cao, G. Lapenta, A combined immersed finite element and conservative semi-Lagrangian scheme for plasma-material interactions, J. Comput. Phys. 488 (2023) 112232.
[50] C. Pagliantini, G. Manzini, O. Koshkarov, G.L. Delzanno, V. Roytershteyn, Energy-conserving explicit and implicit time integration methods for the multi-dimensional Hermite-DG discretization of the Vlasov-Maxwell equations, Comput. Phys. Commun. 284 (2023) 108604.
[51] R. Belaouar, N. Crouseilles, P. Degond, E. Sonnendrücker, An asymptotically stable semi-Lagrangian scheme in the quasi-neutral limit, J. Sci. Comput. 41 (2009) 341–365.
[52] T. Yin, X. Zhong, Y. Wang, Highly efficient energy-conserving moment method for the multi-dimensional Vlasov-Maxwell system, J. Comput. Phys. 475 (2023) 111863.
[53] K. Kormann, E. Sonnendrücker, Energy-conserving time propagation for a structure-preserving particle-in-cell Vlasov–Maxwell solver, J. Comput. Phys. 425 (2021) 109890.
[54] U.S. Inan, M. Gołkowski, Principles of Plasma Physics for Engineers and Scientists, Cambridge University Press, 2010.